Water Resources Management (2023) 37:3527–3542
https://doi.org/10.1007/s11269-023-03512-1

# Investigation of the Different Models of Elliptical-Lopac Gate Performance under Submerged Flow Conditions

**Ashkan Pilbala[1] · Mahmood Shafai Bejestan[2] · Seyed Mohsen Sajjadi[2] · Luigi Fraccarollo[1]**

Received: 21 June 2022 / Accepted: 27 March 2023 / Published online: 18 April 2023


**Abstract**
The effect of the elliptic ratio on the hydraulic performance of the LOPAC gate has been investigated using experimental and Computational Fluid Dynamics *CFD* simulations (Flow-3*D* Hydro). Experiments and simulations were carried out at three different flow discharges, three different submerged ratios, and five different elliptic ratios. In this context, the *CFD* model was first calibrated and verified using the measured data, and then *CFD* simulation was performed. The ratio of upstream/downstream flow depth, the flow discharge coefficient, and the energy dissipation through the gate have been calculated and analyzed, and the three-dimensional features of the flow have been described. Based on the results, the elliptical LOPAC gates with circular weirs determine extreme values of the controlled flow parameters. Asymmetric recirculation downstream of the gate is sometimes observed in the model predictions. The use of Coriolis coefficients relevant to the entire cross-section, here deployed just for the circular and the traditional rectangular Lopac gates, has allowed a concise way to report and compare complex flows for any experimental condition.

**Keywords** Elliptical Lopac gate · Flow-3D · Physical model · Discharge coefficient · Energy dissipation · Coriolis coefficients

## 1 Introduction

It is becoming more necessary for societies to manage water resources more accurately and equitably stirring researchers to seek structures with better and more accurate performance. This can be achieved by optimizing existing structures or by introducing new ones. Several solutions have been introduced and tested to distribute and regulate flow in rivers, such as weirs, sills, embankments, abutments, diversions, sluice or side gates,

✉ Ashkan Pilbala
ashkan.pilbala@unitn.it

[1] Department of Civil, Environmental and Mechanical Engineering, University of Trento, Trento, Italy

[2] Faculty of Water & Environmental Engineering, Shahid Chamran University of Ahvaz, Ahvaz, Iran

etc. It would be difficult, and beyond the purposes of this paper, to summarize the various specific pros and cons of each of them. They interact with morphology, with bio-ecological issues (e.g., fish transit), they involve costs, maintenance, the possibility of maneuver, and changes in their placement, and they behave differently at high and low discharges. Almost all of these aspects still deserve scientific and technical deepening, which may be nowadays faced also through the use of Computational Fluid Dynamics (*CFD*). In fact, recent advances in computer models, besides the boosting up of computer hardware resources, are gaining more and more acceptance as complementary methods for laboratory and field studies.

Gate is one of the hydraulic structures that are used to distribute and regulate the flow discharge and flow depth. There are multiple types of gates, each one having its advantages and disadvantages, and the specific gate type can be selected according to the application (Weyer 2001). Some extensive laboratory studies have been done to show the pros and cons of them (Negm 1998; Negm and Al-Brahim 2002; Akbari et al. 2019; Cox et al. 2015; Salmasi and Abraham 2021) and numerous experimental and numerical studies have been conducted regarding these issues as well (Long et al. 1991; Ferro 2000; Ma et al. 2001; Raiford and Khan 2013, and Gumus et al. 2015; Abhash and Pandey 2021). Long et al. (1991) carried out experiments of submerged jets under sluice gates and compared them in satisfactory way with the numerical results. Ma et al. (2001) also investigated the experimental data of Long et al. (1991) by using a turbulent model in the $2D$ vertical plane. The deviations they observed were attributed to the three-dimensional nature of the flow. The same conclusions, for similar flow conditions, were inferred by Raiford and Khan (2013), who used two models of flow turbulence, the $K-\mathcal{E}$ and the Renormalization group (*RNG*), showing that the *RNG* model gives better vertical profiles of velocity, though both models estimated a water level above the experimental value.

The LOPAC gate, exploited as a flow distribution and regulation structure, gave acceptable performances in executive projects, matching project expectations, such as in the Middle Rio Grande project in New Mexico (Oad and Kinzli 2006). In the 1980s, Peter Langemann designed the LOPAC gate to assist tail end irrigators with balancing fluctuating water supplies. By combining a LOPAC with a hydraulic actuator, Aqua Systems 2000 Inc. (2013) has provided a flexible and economical solution for controlling water in small- and medium-sized canals. After the introduction of the sharp-crested elliptical weir by Cox et al. (2014), the effects of different elliptic ratios on the discharge rate were investigated and relations for the discharge rate were proposed. Afterward, just a few studies have been done on this type of gate. In 2021, Pilbala et al. experimentally studied the elliptical-LOPAC gate (*EL*) with a given shape factor, finding that the discharge coefficient of the flow through the gate in the elliptical case is higher than in the rectangular case. Shafai Bejestan et al. (2020) measured the discharge coefficient associated to the opening of an elliptical Lopac gate gradually converging to the center of channel. Kheybar et al. (2021) used in a laboratory flume a compound structure obtained by installing the Lopac gate at the end of a sudden contraction, made by a short wall orthogonal to the bank. The effects of the presence of the sudden contraction on the discharge coefficient and on energy dissipation have been measured in a set of different opening angles of the Lopac gate, confirming trends already shown by Pilbala et al. (2021) without the sudden contraction.

In all the previous experiments on the elliptical LOPAC gate, only a fixed elliptic ratio (elliptic ratio equal to 1) has been considered. As it happens for the other hydraulic works causing planimetric deviations of riverine flows, such as abutments (Coleman et al. 2005) or bridge piles (Akhlaghi et al. 2019), geometrical changes of the aspect ratio of the Lopac gates have effects on all flow features (on energy dissipation, in particular).

In this study, the primary objective is to investigate gate performance with different elliptical coefficients, submergence ratios, and discharges on the upstream flow depth, discharge coefficient, and energy dissipation.

## 2 Experimental Setup Runs, and Measurements

The experiments were performed in a flume that is 0.8 m wide, 0.8 m high, and 10 m long with a very mild (slightly varying around 0.005) constant longitudinal slope, placed in the hydraulic laboratory of Shahid Chamran University of Ahvaz (Fig. 1). The elliptical ratio of a Lopac gate is defined as the ratio $n = H/W$, as shown in Fig. 1b. The LOPAC gate (Fig. 1) is made of galvanized material with a thickness of 2 mm and is installed at 5 m

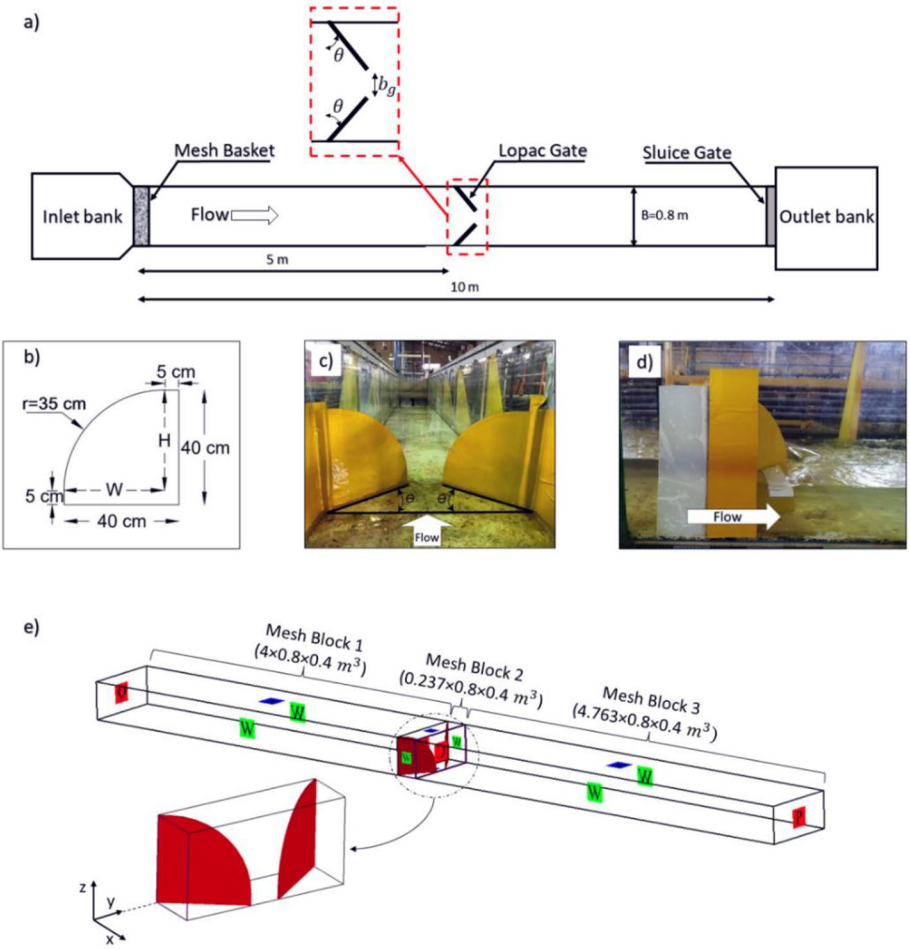


**Fig. 1** **a**) Plan view of the experimental flume, **b**) the dimension of experimental *EL* gate ($n$=1), **c**) the *EL* gate installed in the flume (downstream view), **d**) the *EL* gate installed in the flume (side view), e) mesh generating and boundary conditions of the model

distance from the upstream end. The inlet discharge was measured by an ultrasonic flow meter (Farasanj Abzar CO.LTDUF6001-S / N: 940,088) with an error of 0.1 $l/s$. At the downstream end of the flume, the flow was controlled by a sluice gate mounting a full-width rectangular sharp-edged weir. It permitted to regulate the submerged condition of the gate. A mesh basket was installed at the upstream part of the flume to calm and uniformly distribute the inlet flow. In total, 9 experiments were carried out at three discharges (25, 35, and 45 $l/s$) and three submergence ratios ($S = \frac{y_2}{y_1}$), that are 0.7, 0.8, 0.9. Important enough is where $y_1$ and $y_2$ were measured. The former is taken just upstream of the gate, along the $M_1$ profile taking place there. As it is a slowly varying profile, it does not matter to be precise in the position where to take the measure; we chose to stay about 1 m upstream of the gate. As far as $y_2$ is concerned, it is measured just upstream of the downstream uplifted sluice gate by a point gauge, downstream of the 3$D$ recirculation (shown in Fig. 6) caused by the LOPAC gate. In such a way it is controlled only by the sluice gate opening at a given discharge.

The gate opening angle Θ is set constant at 35 degrees (Fig. 1). In each experiment, after that the discharge is adjusted to the desired value, and the selected submergences were imposed by the sluice gate at the end of the flume. After steady conditions were reached, the measurements were performed using a depth-measuring device at specific points.

Herein we resume the flow variables necessary to describe each run: $Q$ is the discharge, $y_1$ is the water depth upstream of the gate; $y_2$ is the water depth downstream of the gate, $b_g$ is the opening of the gate (Fig. 1), $B$ is the channel width, Θ is the angle of the wings of the gate, $g$ is the acceleration of gravity, $\rho$ is the water-specific mass, $\mu$ is the fluid viscosity, $e_s$ is the roughness of the bed, $s$ is the longitudinal slope. In our experimental and numerical runs, some variables are constant, e.g., $b_g$,$B$ $\Theta$ $s$,$g$,$\rho$,$\mu$,$e_s$. Some of them are set independently of any others, e.g., $Q, y_2, n$. Finally, $y_1$ is just measured, as a result of the configuration the flow reached at steady state. As far as the targets of the paper are concerned, we are interested to evaluate the discharge coefficient $C_d$ of a LOPAC gate and the relative energy dissipation $\frac{\Delta E}{E_1}$ of the flow through the gate, in submerged conditions. These two quantities will be defined later.

We end up with the following expected dependence of the two targeted quantities of this paper:

$$C_d = C_d\left(F_r, Re, n\right) \tag{1}$$

$$\frac{\Delta E}{E_1} = \frac{\Delta E}{E_1}\left(F_r, Re, n\right) \tag{2}$$

where, the Froude number is set as $F_r = Q/\left(By_2\sqrt{gy_2}\right)$, the Reynolds number as $Re = \rho Q/(B\mu)$, $C_d$ is defined in Eq. (4) and $\Delta E = E_1 - E_2$, with $E = \mathrm{y} + \frac{\mathrm{Q}^2}{2g\mathrm{B}^2\mathrm{y}^2}$. The value of $Re$ is varying in a small interval, between 31,250 and 56,250, then the roughness does not play an important role. $F_r$ varies from 0.077 to 0.184, well below unity. This is why we are focusing more on $n$, the effects of which will be shown hereafter.

The governing equation for this type of gate is the energy balance (Eq. 3) between the cross sections where $y_1$ and $y_2$ are measured. Developing it, and using the continuity equation ($Q$ is constant in any cross-section), we obtain Eq. 4, expressing the flow discharge, under submerged and steady flow conditions:

$$y_1 + \frac{\mathrm{Q}^2}{2g\mathrm{B}^2 y_1^2} = y_2 + \frac{\mathrm{Q}^2}{2g\mathrm{B}^2 y_2^2} + \frac{\mathrm{Q}^2}{2g y_2^2}\left(\frac{1}{C_c b_g} - \frac{1}{\mathrm{B}}\right)^2 \tag{3}$$

$$Q = C_d B(y_1 - y_2)\sqrt{2g(y_1 - y_2)} \tag{4}$$

In Eq. 3, $C_c$ is a contraction coefficient. The higher the value of $C_c$ (which is expected to be smaller than unity), the smaller the difference between the area of the vena contracta and the cross-section. $C_d$ in Eq. 4 is directly linked to the coefficient $C_c$ of Eq. 3 through the following Eq. 5.

$$C_d = \left(\frac{1}{1-S}\right)^{1.5}\sqrt{\frac{S^2(\mathrm{S}-1)}{(C_c S)^2 - (C_c b_f)^{-2}}} \tag{5}$$

The experiments are designed to indirectly obtain $C_d$ from Eq. 4, and $C_c$ from Eq. 5. The dependence of $C_d$ on the elliptic shape factor, $n$ is therefore worked out through the dependence of $C_c$ on it.

As a final remark, we emphasize that the size of the laboratory flume implies values of the Reynolds number of the flows we worked with are smaller than those relevant to real cases. On one side this represents a limitation to export and exploit directly our results in the design of real structures. Nevertheless, our aim is to describe and measure the effects on flow induced by different gates under different conditions, so we deem that our results can keep a general validity also in the perspective of real applications.

## 3 Numerical Approach and Runs

A part of the obtained experimental data was first used for calibration and validation of the Flow-3*D* Hydro model Flow Science Inc et al. (2018). The validated model then was executed for different gate geometries and flow conditions to get the final data we needed to complete our analysis. For the calibration stage, the elliptical LOPAC gate with an elliptic ratio equal to 1 was considered, and the three discharge values were run in the experiments. By refining the mesh size and by selecting the turbulence model, the numerical model was calibrated so that the results of the simulation were mesh independent and compared well with the measured values of water level within the required accuracy. Subsequently, further four LOPAC gates with elliptic ratios ($n = H/W$) equal to 0.5 ($n = \frac{0.175}{0.35}$), 0.7($n = \frac{0.245}{0.35}$), 1.3($n = \frac{0.35}{0.2692}$), and 1.5($n = \frac{0.35}{0.2333}$), were simulated under three different flow conditions (the three discharges 25, 35, and 45 $l/s$) and three submergence ratios ($S = 0.7$, 0.8, and 0.9), so in total, 45 simulations were performed to figure out the different models of *EL* gate performance under submerged flow conditions.

### 3.1 Turbulence Closures

In this study, four turbulence models of *RNG*, $K-\mathcal{E}$, $K-\omega$, and Large Eddy Simulation (*LES*) have been used to measure their accuracy in estimating the characteristics of flow through the *EL* gate. The equations of *RNG* and $K-\mathcal{E}$ models are similar; however, equation constants are found empirically in the standard $K-\mathcal{E}$ model and explicitly in the *RNG* model. The *RNG* model is known to describe low-intensity turbulence and flows having

strong shear regions more accurately than the standard $K-\mathcal{E}$ model, so the former model has wider applicability. The $K-\omega$ model is deemed to be accurate in particular to describe flow domains near wall boundaries and flows with streamwise pressure gradients, like jets and wakes. In the *LES* model, the effects of small scale turbulence are represented by an eddy viscosity. In this study, in Section 4.1, all these turbulence models have been exploited and compared.

### 3.2 Mesh Generation and Boundary Conditions

Three mesh blocks (the first mesh block upstream of the gate, the middle mesh block around the LOPAC gate, and the final one downstream of it) (Fig. 1e) have been employed. The mesh dimension is constant throughout any block, and it is the same in the first and third blocks, whereas it is constant but finer in the second block. The mesh sizes, the large and the small ones have been determined based on three criteria: simulation time, error rate, and capabilities of the applied software/hardware. The extension of the first, second, and third blocks, in the $x$, $y$, and $z$ directions, are $4\times0.8\times0.4$, $0.237\times0.8\times0.4$, and $4.763\times0.8\times0.4\ m^3$, respectively (Fig. 1e).

The boundary conditions used in the model consisted of imposing the flow discharge at the upstream cross-section and the flow depth at the downstream cross-section. In both boundaries, the pressure has been distributed according to the hydrostatic assumption. Moreover, the common boundaries of the mesh blocks were of the (or transmissive) type; floor boundaries and all the flume walls were selected to be of the wall type; and the free surface was of the symmetry type with a null relative pressure (Fig. 1e).

### 3.3 The Sensitivity Analysis of the Mesh Resolution

A mandatory choice in the numerical analysis concerns the mesh accuracy, or, in other words, the independency of the results on the mesh size. We did some preliminary work devoted to selecting the optimum size of the cells that allowed us to get results that are mesh-independent within an assigned error. In this study, we evaluated 3 different mesh sizes ($M0$, $M1$, and $M2$) to assess the mesh size. In all cases, the adopted turbulent model was $RNG$, which, as described hereafter, was selected among the other ones. In each mesh, the cells in blocks 1 and 3 are the same, whereas, in mesh block number 2, which contains the gate, the cells are finer. The cell size of mesh blocks 1 and 2 for M0 were $\Delta x=\Delta y=\Delta z=0.02695$ m and $\Delta x=\Delta y=\Delta z=0.00667$ m, for M1 $\Delta x=\Delta y=\Delta z=0.0245$ m and $\Delta x=\Delta y=\Delta z=0.0061$ m, and finally, for M2, $\Delta x=\Delta y=\Delta z=0.02205$ m and $\Delta x=\Delta y=\Delta z=0.00554$ m. The results have shown that $M1$ mesh, compared with $M0$, gives results with a relative error greater than 0.1% (0.424), while, comparing $M2$ and $M1$, the relative error, is smaller than 0.1% (0.083). $M1$, therefore, has been chosen for the simulation with the total number of cells being less than 500,000 cells.

## 4 Results and Analysis

### 4.1 Choice of the Turbulent Model and Validation

The results of the numerical simulations of the Elliptical-LOPAC gate with an ellipticity ratio $n = 1$, in comparison with the experimental data, is generally satisfying for all four turbulence closures. Table 1 shows the error rate for various criteria, *RMSE* (Root Mean Square Error); $MAPE$ (Mean absolute percentage error); *RE* (relative error); *MAD* (Median absolute deviation); and *MSE* (Mean squared error), applied to flow depths at three specified points (upstream, on the gate, and downstream of the LOPAC-elliptical gate), against the relevant measured data, for the various turbulent models in runs at a discharge of 45 $l/s$ and three submergence ratios. Results show that among the different turbulence models, the best performance, in comparison with the measured flume data, was obtained by the *RNG* and $K-\mathcal{E}$ models; $RNG$ was chosen for the rest of the runs. To validate the *RNG* model, we then exploited it also in the simulation of the flow through the Elliptical-LOPAC gate for another discharge rate, which is $Q = 25l/s$, and the results were in an acceptable range of errors. Hence, in the end, the *RNG* model was selected to simulate all the cases, also those for which relevant experimental data are not available.

### 4.2 Free Surface Profiles Along the Flume for the Various Elliptic Ratios ($n$) of the Lopac Gates

One of the criteria for assessing the effects induced on the flow by different gate types is by checking the value of the upstream depth. The higher variations of the upstream depths associated with given variations of the discharge, keeping constant $y_2$, the more accurate is the use of the characteristic law (Eq. 4) to calculate the discharge (i.e., the depth measurement error rate is less). We have exploited the *CFD* results to observe how the elliptic ratios $n$ are affecting the submergence ratios, keeping constant the downstream depth $y_2$. Figure 2 illustrates the calculated longitudinal profiles of the flow for different elliptic ratios ($n$). In these Figures, we represent the profile just in a reach from 1 m upstream till 4 m downstream of the gate (placed at $x = 0$ in the Figures), along the longitudinal symmetric axis; out of this reach the profile is about uniform. The profiles in Fig. 2 indicate that elliptical Lopac gates with elliptic ratios $n$ less than 1 ($n < 1$) have a better performance because they present higher flow depths ($y_1$) upstream of the gate (e.g., with $Q = 45l/s$, $y_1 = 0.37$ m at $n = 0.5$, $y_1 = 0.35$ m at $n = 1$ and $y_1 = 0.357$ m at $n = 1.5$).

The dependence of $y_1$ on $n$, at given flow conditions (same $Q$ and $S$) is monotonously decreasing as $n$ increases in the range $n < 1$ whereas the opposite takes place for $n > 1$. Furthermore, the rate of change of $y_1$ with n, is greater for n less than 1. Hence, gates with elliptic ratios with $n = 1$ have the least effects on the increase of the flow head upstream of the gate, whereas gates with elliptic ratios smaller than 1 have shown the best performance in enhancing the flow depth $y_2$, upstream of the gate.

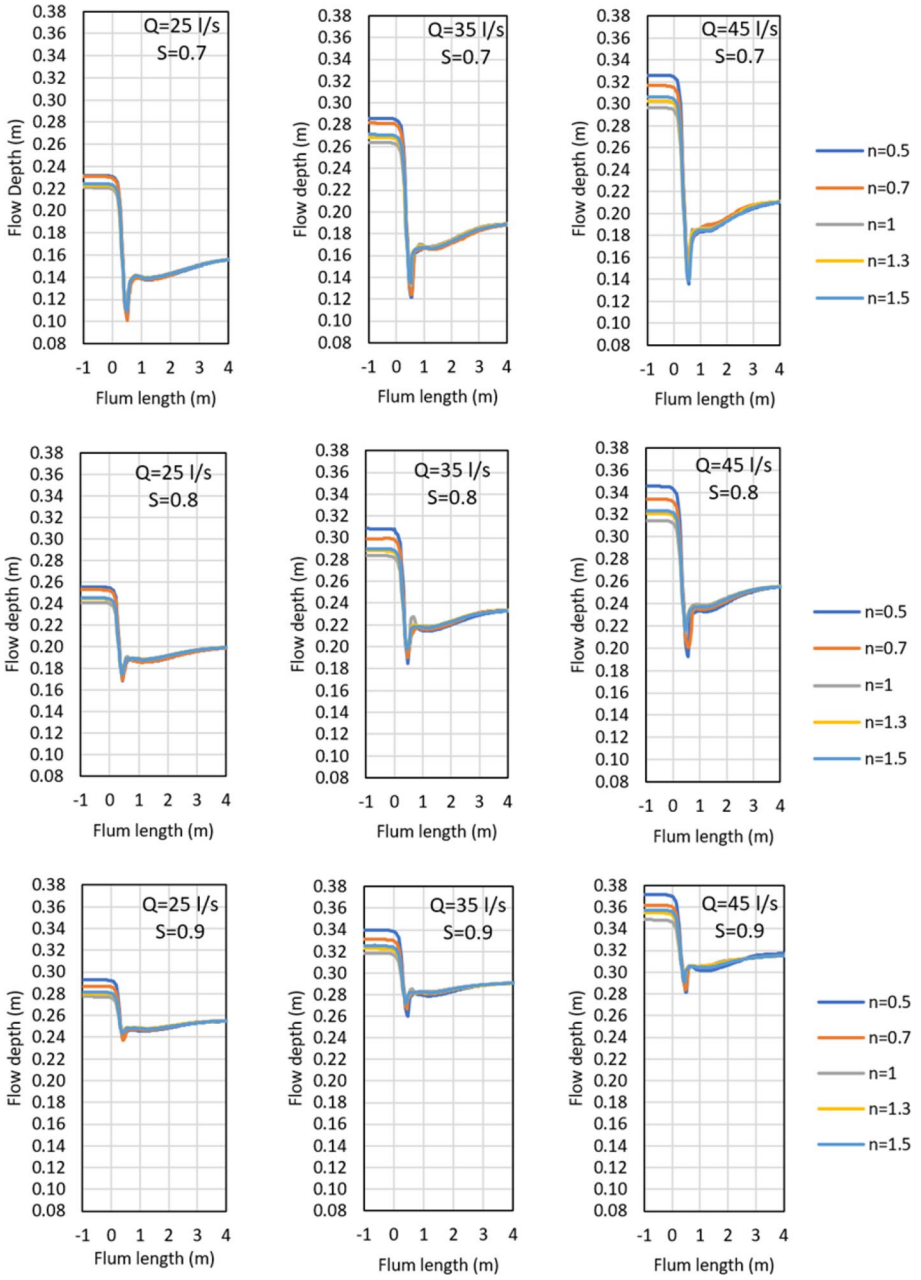


**Fig. 2** Elliptic ratio effect on water depth

### 4.3 Coriolis' Coefficient ($\alpha$, $\beta$)

Equations 6 and 7 report the well-known Coriolis compensations coefficients, $\beta$, and $\alpha$, that are used to express the flux of momentum and mechanical energy, respectively, in terms

**Table 1** Statistical results of the simulation turbulence model ($n = 1$) with the laboratory model (Lab) at a discharge of 45 ($l/s$) at three control points

| Θ(°) | Q(l/s) | S | T-model | $y_1$(m) | y(gate) (m) | $y_2$(m) | RMSE(m) | MAPE(%) | RE(%) | MAD(%) | MSE(%) |
|---|---|---|---|---|---|---|---|---|---|---|---|
| 35 | 45 | 0.7 | Lab | 0.302 | 0.268 | 0.211 | | | | | |
| | | | RNG | 0.297 | 0.267 | 0.211 | 0.0033 | 0.7926 | 1.8531 | 0.2300 | 0.0011 |
| | | | *K–ℰ* | 0.297 | 0.267 | 0.211 | 0.0033 | 0.8490 | 1.8531 | 0.2433 | 0.0011 |
| | | | K-ω | 0.294 | 0.266 | 0.212 | 0.0048 | 1.1560 | 2.6473 | 0.3400 | 0.0023 |
| | | | LES | 0.296 | 0.267 | 0.211 | 0.0039 | 0.9875 | 2.1840 | 0.2833 | 0.0015 |
| | | 0.8 | Lab | 0.320 | 0.288 | 0.256 | | | | | |
| | | | RNG | 0.315 | 0.287 | 0.256 | 0.0031 | 0.6998 | 1.6250 | 0.2177 | 0.0009 |
| | | | *K–ℰ* | 0.316 | 0.289 | 0.255 | 0.0022 | 0.5641 | 1.1562 | 0.1723 | 0.0005 |
| | | | K-ω | 0.318 | 0.290 | 0.255 | 0.0018 | 0.6057 | 0.6562 | 0.1757 | 0.0003 |
| | | | LES | 0.317 | 0.289 | 0.255 | 0.0019 | 0.5991 | 0.8750 | 0.1757 | 0.0004 |
| | | 0.9 | Lab | 0.351 | 0.326 | 0.315 | | | | | |
| | | | RNG | 0.349 | 0.326 | 0.316 | 0.0013 | 0.2705 | 0.6553 | 0.0933 | 0.0002 |
| | | | *K–ℰ* | 0.349 | 0.327 | 0.315 | 0.0016 | 0.4139 | 0.7123 | 0.1400 | 0.0003 |
| | | | K-ω | 0.349 | 0.328 | 0.316 | 0.0020 | 0.5264 | -0.7055 | 0.1767 | 0.0004 |
| | | | LES | 0.349 | 0.328 | 0.315 | 0.0015 | 0.3972 | -0.5521 | 0.1333 | 0.0002 |

of cross-section, and averaged velocity. Hence, their behaviors are a function of the longitudinal position, only, and reflect the variations of velocities and depths across the flow section, lumping in the strong three-dimensional features induced by the gate. In particular, they take into account the asymmetries of the flow observed in the recirculating zones, downstream of the gate, and the flux overtopping the curved, sharp-crested weir of the Lopac gate. It is also reasonable and confirmed by the results, that the higher the Coriolis coefficients are around the gate, the higher the energy dissipation will be. All the results we present are obtained by running the Flow-3*D* code.

$$\beta = \frac{\int_A u^2 dA}{U^2 A} \tag{6}$$

$$\alpha = \frac{\int_A u^3 dA}{U^3 A} \tag{7}$$

In Fig. 3a, b it is the role of the elliptic coefficient n on $\alpha$ and $\beta$ to be focused on. We see that n = 1 presents the lowest values of $\alpha$ and $\beta$ throughout the flow domain. To highlight the role of the flow overtopping the weir we compare the *EL* gate with a traditional rectangular Lopac (*RL*) gate (Pilbala et al. 2021) which conveys the flow between its vertical sides. In this case, the contraction of the vena downstream of the gate is more pronounced than for a Lopac gate. In the comparison, we changed only the shape of the gate, while all the other parameters (i.e., the flow discharge, the width of the gate and the channel, the depth $y_2$, etc.) are the same. The results, reported in Figs. 3c, d, indicate that the $y_1$ depth is higher for the rectangular gate, and so is therefore also the energy dissipation of the flow through the gate. Accordingly, the Coriolis coefficients are higher for the rectangular gate, being the difference between the *RL* and *EL* gates bigger when the submergence is higher.

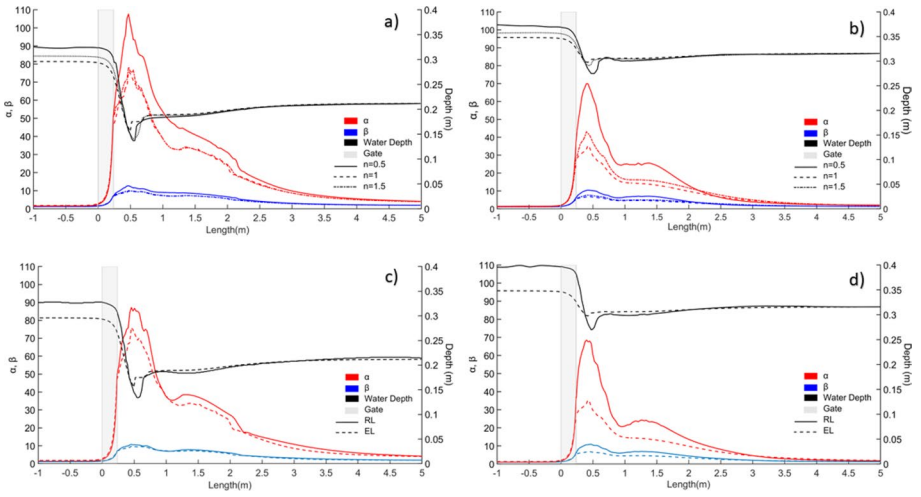


**Fig. 3** Coriolis longitudinal profiles: a) $S = 0.7$ and b) $S = 0.9$ for different elliptic ratios and constant discharge ($Q = 45l/s$) c) $S = 0.7$ and d) $S = 0.9$ for the *RL* and the *EL* gate ($n = 1$) gate, with assigned $Q$

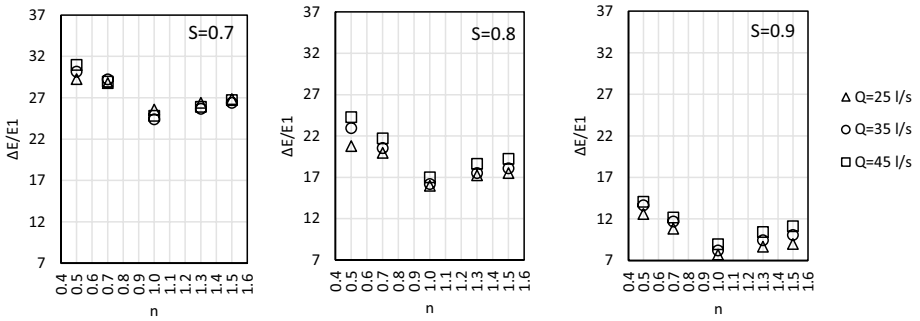


**Fig. 4** Elliptic ratio effects on energy dissipation

### 4.4 Elliptic Ratio Effect on Energy Dissipation (*E*)

The relative flow energy dissipation, $\Delta E = \frac{E_1 - E_2}{E_1}$, is important to characterize the flow behavior around Lopac gates and to direct the gate selection. $E_1$ is the Energy before the gate ($E_1 = y_1 + \alpha_1 \frac{V_1^2}{2g}$) and $E_2$ is Energy after the gate ($E_2 = y_2 + \alpha_2 \frac{V_2^2}{2g}$). As shown in Fig. 4, for a certain type of gate (given $n$), the relative energy dissipation decreases with $S$. This can be explained by observing that by increasing the submergence ratios $S$, the Froude number of the flow in front of the gate decreases; hence, a smaller amount of kinetic energy to be dissipated through the gate is available. The reference gate ($n = 1$) allows a minimum energy dissipation in all flow conditions, as displayed in Fig. 4. An explanation of this effect is not straightforward, but quite important as a criterion to select the gate.

We already know (Pilbala et al. 2021) that the circular gate profile ($n = 1$) allows more friendly management than the rectangular ($n \to \infty$) one. In this study, we see (Fig. 4) that $n = 1$ corresponds to the minimum relative energy dissipation independently of $Q$ and $S$. In particular, the minimum relative energy dissipation, obtained with $n = 1$, submergence ratio 0.9, and $Q = 25 l/s$ the (minimum) ($\Delta E$), was equal to 7.6%. Vice versa, the highest energy loss was around 31%, reached with $n = 0.5$, submergence ratio 0.7, and $Q = 45 l/s$ (Fig. 4). Furthermore, we observe that the gates with $n = 0.5$ and $n = 0.7$ have always dissipated more relative energy than the cases $n = 1.3$ and $n = 1.5$. The role of $Q$ in the value of relative dissipation is generally less important than that caused by $S$ and $n$.

### 4.5 Elliptic Ratios Effect on Energy Dissipation Coefficient ($C_c$) and Discharge Coefficient ($C_d$)

This section is aimed at investigating the effect of different elliptic ratios $n$ on contraction coefficient and discharge coefficient, $C_c$ and $C_d$, respectively. $C_c$, defined by Eqs. 4 and 5, as above highlighted, is also connected to the amount of energy dissipation. This coefficient is close to 1, with small variations as $Q$ varies (Fig. 5), meaning that the model choice for the local (Borda type) energy dissipation is quite appropriate. According to Fig. 5, the large variation of $C_c$, from the minimum and maximum discharge, is relevant to the gate with $n = 0.5$ and $S = 0.9$. By the three panels of Fig. 5, we can also appreciate that $S = 0.9$ determines the largest deviations from unity, as $Q$ varies.

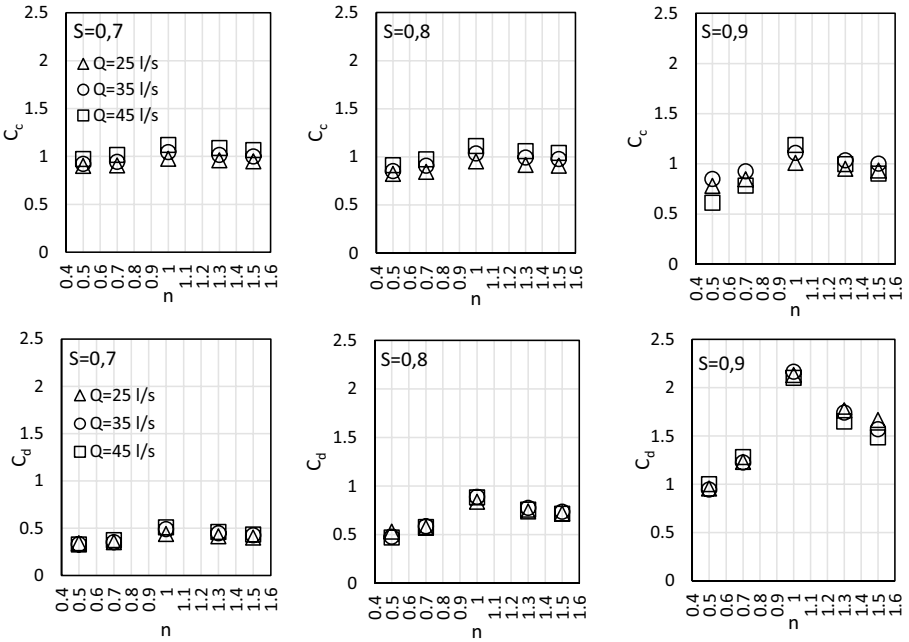


**Fig. 5** Elliptic ratio Effect on $C_d$

The discharge coefficient, $C_d$, defined in Eqs. 4 and 5, represents a specific coefficient of the discharge passing through the gate. Equation 5 actually consists of a characteristic formula to evaluate the discharge and has a prominent role in classifying the hydraulic performance of the gate. As mentioned in the previous section, the gate model $n = 1$ has created the lowest increment of the upstream head, which means that it allows the passage of a flow with the highest discharge compared to *EL* gates with any other value of $n$. Figure 5 shows all this and presents $C_d$ values that, though depending on $C_c$ (Eqs. 4 and 5), have variations with $Q$, generally smaller than the corresponding variations of the $C_c$ values. This is quite good as far as the easiness and accuracy of this evaluation formula are concerned. In particular, with $n = 1$, the values of $C_d$ are about 0.5, close to 1, and slightly higher than 2.1 for submergence ratios $S$ equal to 0.7, 0.8, and 0.9, respectively (Fig. 5). Also, this figure illustrates that the discharge coefficients obtained with $n < 1$ are smaller than those obtained with $n > 1$, at all $S$ ($S = 0.7, 0.8, 0.9$). *EL* with $n = 1$, therefore, confirms to be a reference among the other *EL*, as it was associated with the maximum or minimum value of any parameter involved in the phenomenon.

### 4.6 Three-dimensional Flow Pattern in the Gate Range

The simulations of the elliptical LOPAC gate show that, at all discharges and submergence ratios, in the contraction area after the gate, the lowest velocities are displayed for the case $n = 1$, the highest velocities for $n < 1$, as reported in Fig. 6a. It also shows the vortices forming downstream of the Lopac gates, at $n = 0.5$, 1, and 1.5, on both sides of the flume. These vortices are quite similar, but not identical, for the three gates. The stagnant water

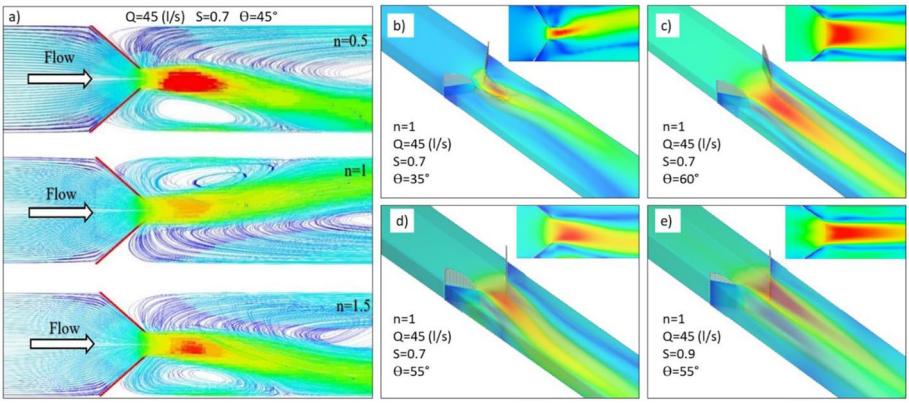


**Fig. 6** **a**) Form of vortices behind the gates (Top view); the effect of opening angle on symmetry for *EL* gate (**b** and **c**); the effect of submerge ratio on symmetry for *EL* gate (**d** and **e**)

space behind the gate is a suitable space for sediment deposition or algae and straw growth. Our results indicate that the stagnant water space area behind the gate with an elliptic ratio 0.5 has the minimum extension.

An important aspect, which somehow unexpectedly came out from most of the simulation, is the asymmetric feature. This is not triggered by the geometry, boundary, or initial conditions, which all would favor a symmetric solution. The simulation starts from an arbitrary symmetric initial condition, which is not important for the analysis. Later on, the flow autonomously evolves toward its final configuration, which could be steady or not, and, if not, periodic (Varchanis et al. 2020, Williamson and Brown 1998, Tavelli and Dumbser 2014) or chaotic. From the observation of the movies that present the predicted evolution in time of the flow, we observed that the flow reaches, in all conditions, a steady state, independently of the initial conditions. Furthermore, we see that the flow may deviate, downstream of the gate, toward either side of the channel, whereas it keeps the symmetry upstream of the gate and also inside it. Figure 6 clearly illustrates this issue. Boundary and initial conditions are not playing a role in this outcome, as is proven by the fact that in some runs the symmetric configuration of the flow is maintained. We are deeming this feature is interesting and important to be reported, and we are aware that it could be responsible for some consequences; for instance, the stress field around one bank is increased compared to the symmetric solution. We also wonder whether some sediment transport would create positive or negative feedback, contributing to enhancing or damping the flow deviations.

From our runs, we saw that there are conditions that permit to achieve symmetric numerical solutions. One of these is the case with a wide enough opening angle, and another one is the case with a high enough submergence ratio. An increase of the angle (and so of the width at the end of the gate) or an increase of the submergence ratio, favor the maintenance of a symmetric solution, from the start of the simulation till the reaching of its final steady state. Figure 6 illustrate this point. In particular, Fig. 6b, c compare the steady solution for the case of two gate angles, given all the other quantities (discharge, submergence, type of gate, bed slope, channel width, roughness, etc.), while in Fig. 6d, e are the submergence rate to vary.

Given the computational effort required for a single run and the amount of quantities to tune (including here also the turbulent model), it has not been possible to go further in the

analysis of the setting allowing or not a symmetric solution. All this acknowledged, it was not even the focus of this work to go in-depth and enlighten the mathematical/numerical origins of the asymmetry.

## 5 Conclusion

The Elliptical LOPAC gate, introduced in 2021, can be considered as a new generation of weir-gates, with specific performance features, to be used for the management of irrigation canals. In this study, using laboratory information and *CFD* code, the elliptic ratio effect of elliptical LOPAC gates on the upstream flow control, discharge coefficient, and energy dissipation of the flow through the gate were evaluated. The following items can be mentioned as key research results:

1. Elliptic ratios $n$ less than 1 ($n = 0.5, n = 0.7$) yield higher values of the flow depth in the upstream flow than ratios $n$ larger than 1 ($n = 1.3, n = 1.5$); the lowest upstream flow depth was obtained with the elliptic ratio $n = 1$.
2. The highest discharge coefficient ($C_d$=2.1) was obtained for the elliptic ratio 1 and the minimum was $C_d$=0.3 for the elliptic ratio 0.5. The results show that elliptic ratios greater than 1 ($n = 1.3, n = 1.5$) determine a higher discharge coefficient than ratios $n$ smaller than 1 ($n = 0.5, n = 0.7$).
3. The lowest relative energy dissipation rate (i.e., 7.9%) was obtained for the gate with the elliptic ratio $n = 1$. The energy dissipation of the EL gates with $n$ less than 1 ($n = 0.5, n = 0.7$) is higher than the energy dissipation of EL gates with $n$ larger than 1($n = 1.3, n = 1.5$);
4. Steady symmetric or non-symmetric recirculating flows, downstream of the Lopac gate, have been predicted by the numerical solutions. An increase of the $b_g/B$ ratio, or an increase of the submergence ratios, favors the maintenance of a symmetric steady solution.
5. By exploiting a formulation of the Coriolis compensation coefficients for the momentum and the mechanical energy fluxes ($\alpha$ and $\beta$, respectively) involving the entire cross-section, we found a way to lump into single parameters the complex three-dimensional features of the flow, especially around and immediately downstream of the gate. Compared to rectangular gates, the ellipticity of the shape for the gate with $n = 1$ allows a reduction of the values of the Coriolis coefficients throughout the flow domain. Also, among elliptical the Lopac gates, $n = 1$ yields the lowest values of $\alpha$ and $\beta$, which is consistent with the energy dissipation rates above presented and discussed.

**Acknowledgements** We are grateful to the Research Council of Shahid Chamran University of Ahvaz for financial support (GN:SCU.WH98.343) and the support of Italian PRIN 2017 project Enterprising (2017SEB7Z8). Simulation result courtesy of Flow Science, Inc., developer of the computational fluid dynamics (*CFD*) software, FLOW-3D® (https://www.flow3d.com). We would like to express our very great appreciation to Mr. Stefano Mascetti and Mr. Filippo Palo from *XC* Engineering Srl Company for their valuable and constructive suggestions during the simulation of this research work.

**Author Contributions** The first author contributed to all parts of this study (experiments in the lab, numerical simulations, data analysis, and writing), the second and third authors contributed to the experimental investigation at the Hydraulic Laboratory of Shahid Chamran University of Ahvaz, Iran, and also data analyzing, and writing. The last author contributed to numerical simulations, data analysis, and writing. All authors read and approved the final manuscript.

**Funding** Open access funding provided by Università degli Studi di Trento within the CRUI-CARE Agreement.

- We are grateful to the Research Council of Shahid Chamran University of Ahvaz for financial support (GN:SCU.WH98.343).
- This work has been supported by the Italian PRIN 2017 project Enterprising (2017SEB7Z8).
- Simulation result courtesy of Flow Science, Inc., developer of the computational fluid dynamics (CFD) software, FLOW-3D® (https://www.flow3d.com).

**Data Availability** The data and code that support the study are available from the corresponding author upon reasonable request.

## Declarations

**Competing Interests** All authors declare they have no financial interests.



## References

Aqua Systems 2000 Incorporation (AS21) (2013) Leaders in Water Management and Control. http://www.as2i.net/products/control-gates/hydra-lopac-gate

Abhash A, Pandey KK (2021) Experimental and Numerical Study of Discharge Capacity and Sediment Profile Upstream of Piano Key Weirs with Different Plan Geometries. Water Resour Manag 35:1529–1546. https://doi.org/10.1007/s11269-021-02800-y

Akbari M, Salmasi F, Arvanaghi H et al (2019) Application of Gaussian Process Regression Model to Predict Discharge Coefficient of Gated Piano Key Weir. Water Resour Manag 33:3929–3947. https://doi.org/10.1007/s11269-019-02343-3

Akhlaghi E, Babarsad SM, Derikvan E (2019) Abedini M (2019) Assessment the Effects of Different Parameters to Rate Scour around Single Piers and Pile Groups: A Review. Arch Comput Methods Eng 27:183–197. https://doi.org/10.1007/s11831-018-09304-w

Cox LA, Kullberg EG, Mackenzie KA, Thornton CI (2014) Stage -Discharge Rating Equation for an Elliptical Sharp-Crested Weir. J Irrig Drain Eng 140(6):040014018. https://doi.org/10.1061/(ASCE)IR.1943-4774.0000730

Cox LA, Saadat S, Mackenzie KA, Thornton CI (2015) Effect of Urban Debris on Hydraulic Efficiency of an Elliptical Sharp-Crested Weir. J Irrig Drain Eng 141(6):06014006. https://doi.org/10.1061/(ASCE)IR.1943-4774.0000837

Coleman S, Lauchlan C, Melville B (2005) Clear-water scour development at bridge abutments. J Hydraul Res IAHR 43(4):445–448. https://doi.org/10.1080/00221680509500142

Ferro V (2000) Simultaneous flow over and under Gate. J Irrig Drain Eng 126(3):190–193. https://doi.org/10.1061/(ASCE)0733-9437(2000)126:3(190)

Flow Science, Inc., Santa Fe, NM, USA. ***FLOW-3D***® Version 12.0 User's Manual (2018) [Online]. Accessed on: Feb. 3, 2019

Gumus V, Simsek O, Soydan N, Akoz M, Kirkgoz M (2015) Numerical modeling of submerged hydraulic jump from a sluice gate. J Irrig Drain Eng. https://doi.org/10.1061/(ASCE)IR.1943-4774.0000948

Kheybar H, Sajjadi S M, Ahadyan (2021) Effect of sudden canal contraction on the discharge coefficient and the energy dissipation coefficient of the elliptical LOPAC gate. Irr Drain J:1–10. https://doi.org/10.1002/ird.2622

Long D, Steffler PM, Rajaratnam N (1991) A numerical study of submerged hydraulic jumps. J Hydraul Res 29(3):293–308. https://doi.org/10.1080/00221689109498435

Ma F, Hou Y, Prinos P (2001) Numerical calculation of submerged hydraulic jumps. J Hydraul Res 39(5):493–503. https://doi.org/10.1080/00221686.2001.9628274

Negm AM (1998) Characteristics of Combined Flow over Weirs and under Gates with Unequal Contractions. In Advances in Hydroscience and Engineering, Vol.2, Part A, (Edited by CHES and IRTCES, Proc.2nd ICHE-95, 22–26 March)

Negm AM, Al-Brahim AM (2002) AlHamid A A (2002) Combined free flow over weirs and below gates. J Hydraul Res 40(3):359–365. https://doi.org/10.1080/00221680209499950

Oad R, Kinzli K (2006) SCADA Employed in Middle Rio Grand Vally to Help Deliver Water Efficiently. News Letter of the water center at Colorado State University. https://as2i.net/products/

Pilbala A, Sajjadi SM, ShafaiBejestan M (2021) Hydraulic Performance of Elliptical-Lopac Gate under Submerged Flow Conditions. Ain Shams Eng J 12(1):317–326. https://doi.org/10.1016/j.asej.2020.05.007

Raiford JP, Khan AA (2013) Turbulence schemes for modeling a submerged hydraulic jump. Eng Comp Mech 166(EM1):40–51. https://doi.org/10.1680/eacm.11.00003

Salmasi F, Abraham J (2021) Prediction of discharge coefficients for sluice gates equipped with different geometric sills under the gate using multiple non-linear regression (MNLR). J Hydrol 597:125728. https://doi.org/10.1016/j.jhydrol.2020.125728

Shafai Bejestan M, Zeinivand M, Tahmasebi poor M (2020) Discharge Coefficient of Elliptical Lopac Gate with Gradual Transition in Submergence Condition. J Hydraul 15(2):67–80. https://doi.org/10.30482/jhyd.2020.225028.1449

Tavelli M, Dumbser MA (2014) Staggered semi-implicit discontinuous Galerkin method for the two-dimensional incompressible Navier-Stokes equations. Appl Math Comput 248:70–92. https://doi.org/10.1016/j.amc.2014.09.089

Varchanis S, Hopkins CC, Shen QA, Tsamopoulos J, Haward JS (2020) Asymmetric flows of complex fluids past confined cylinders: A comprehensive numerical study with experimental validation. Phys Fluids 32(053103):1–18. https://doi.org/10.1063/5.0008783

Weyer E (2001) System identification of an open water channel. Control Eng Pract 9(12):1289–1299. https://doi.org/10.1016/S0967-0661(01)00099-5

Williamson CHK, Brown GL (1998) A Series in $1/\sqrt{\text{Re}}$ to Represent the Strouhal-Reynolds Number Relationship of the Cylinder Wake. J Fluids Struct 12(8):1073–1089. https://doi.org/10.1006/jfls.1998.0184